Neuroscience 205 (2012) 140–153

MORPHOMETRIC VARIABILITY OF NICOTINAMIDE ADENINE DINUCLEOTIDE PHOSPHATE DIAPHORASE NEURONS IN THE PRIMARY SENSORY AREAS OF THE RAT

M. A. M. FREIRE,[a,b] J. FABER,[b1] C. W. PICANÇO-DINIZ,[a] J. G. FRANCA[c] AND A. PEREIRA[d*]

[a]*Laboratory of Neurodegeneration and Infection, João de Barros Barreto Universitary Hospital, Federal University of Pará, 66073-000 Belém, PA, Brazil*

[b]*Edmond and Lily Safra International Institute for Neurosciences of Natal, 59066-060 Natal, RN, Brazil*

[c]*Instituto de Biofísica Carlos Chagas Filho, Universidade Federal do Rio de Janeiro, 21941-902 Rio de Janeiro, RJ, Brazil*

[d]*Brain Institute, Federal University of Rio Grande do Norte, 59056-450 Natal, RN, Brazil*

Abstract—Even though there is great regional variation in the distribution of inhibitory neurons in the mammalian isocortex, relatively little is known about their morphological differences across areal borders. To obtain a better understanding of particularities of inhibitory circuits in cortical areas that correspond to different sensory modalities, we investigated the morphometric differences of a subset of inhibitory neurons reactive to the enzyme nicotinamide adenine dinucleotide phosphate diaphorase (NADPH-d) within the primary auditory (A1), somatosensory (S1), and visual (V1) areas of the rat. One hundred and twenty NADPH-d–reactive neurons from cortical layer IV (40 cells in each cortical area) were reconstructed using the Neurolucida system. We collected morphometric data on cell body area, dendritic field area, number of dendrites per branching order, total dendritic length, dendritic complexity (Sholl analysis), and fractal dimension. To characterize different cell groups based on morphology, we performed a cluster analysis based on the previously mentioned parameters and searched for correlations among these variables. Morphometric analysis of NADPH-d neurons allowed us to distinguish three groups of cells, corresponding to the three analyzed areas. S1 neurons have a higher morphological complexity than those found in both A1 and V1. The difference among these groups, based on cluster analysis, was mainly related to the size and complexity of dendritic branching. A principal component analysis (PCA) applied to the data showed that area of dendritic field and fractal dimension are the parameters mostly responsible for dataset variance among the three areas. Our results suggest that the nitrergic cortical circuitry of primary sensory areas of the rat is differentially specialized, probably reflecting peculiarities of both habit and behavior of the species.

Key words: circuitry, inhibitory neurons, morphometry, primary areas, rat.

Since Santiago Ramón y Cajal, the neuron is considered the elementary unit of the brain (Shepherd, 1991). The view of the neocortex as a uniform structure, being composed of the same neuronal modules distributed along its surface, has held its appeal for many years (Szentágothai, 1978; Rockel et al., 1980), even with early evidence pointing to a noticeable variation in regional and species structure mainly of excitatory neurons (DeFelipe and Jones, 1988). Despite many setbacks, the search for such a canonical microcircuit arranged along the cortex with crystalline regularity has persisted (Douglas and Martin, 2007). Lately, though, evidence has shown systematic regional differences in cell density across cortical areas and species (Collins et al., 2010) and also in the morphological organization of both excitatory (Jacobs et al., 2001; Elston et al., 2005, 2006a) and inhibitory cortical circuits (Bidmon et al., 1997; Somogyi et al., 1998; Barone and Kennedy, 2000; Freire et al., 2007). Pyramidal cells, for instance, which comprise more than 70% of the neurons in the cerebral cortex (DeFelipe and Fariñas, 1992), differ in size, branching pattern, and number of dendritic spines in distinct cortical areas (Elston, 2002, 2003). This has been observed in rodent (Benavides-Piccione et al., 2006; Elston et al., 2006b; Chen et al., 2009) and primate species (Elston et al., 2006a), including humans (Jacobs et al., 2001).

Similar to pyramidal cells, inhibitory neurons are heterogeneously distributed across distinct cortical regions as well (DeFelipe, 1993a, 1997), acting as modulators/inhibitors of brain activity, contributing to regional differences in cortical function (DeFelipe, 2002). A very simple and robust technique, nicotinamide adenine dinucleotide phosphate diaphorase (NADPH-d) histochemistry (Thomas and Pearse, 1964), reveals a subset of GABAergic interneurons (Valtschanoff et al., 1993), corresponding to nearly 2% of the entire pool of cortical neurons (Gabbott and Bacon, 1995). NADPH-d cells coexpress differentially other substances in the rodent cortex, such as somatostatin, neuropeptide Y (NPY), substance P (Aoki and Pickel, 1990; Gonchar et al., 2007; Kubota et al., 2011), and the calcium-binding proteins calbindin, calretinin, and parvalbumin (Lee et al., 2004; Lee and Jeon, 2005), although such colocalization seems to vary depending on the species and the cortical area evaluated (Druga, 2009). In addition, these neurons are an important source of nitric

[1] Present address: Department of Informatics and Computational Sciences, Federal University of Latin American Integration - UNILA, 85856-970 Foz do Iguaçu, PR, Brazil.
*Corresponding author. Tel: +55-84-9193-6311.
E-mail address: apereira@ufrnet.br (A. Pereira).

Abbreviations: A1, primary auditory cortex; PB, phosphate buffer; PCA, principal component analysis; NADPH-d, NADPH diaphorase; NO, nitric oxide; NOS, nitric oxide synthase; S1, primary somatosensory cortex; V1, primary visual cortex.

0306-4522/12 $36.00 © 2011 IBRO. Published by Elsevier Ltd. All rights reserved.
doi:10.1016/j.neuroscience.2011.12.029

oxide (NO), given the well-documented colocalization between NADPH-d and nitric oxide synthase (NOS) enzymes in the brain (Dawson et al., 1991; Hope et al., 1991). According to their morphological characteristics, NADPH-d cells can be further divided into two subgroups, based mainly in the appearance of the dendritic tree: type I cells, which possess large cell bodies and a heavily stained dendritic tree, and type II cells, smaller and devoid of visible dendrites (Lüth et al., 1994; Sandell, 1986; Freire et al., 2004).

Despite prior investigations of the areal distribution of NADPH-d neurons (Sandell, 1986; Yan et al., 1996; Franca et al., 1997, 2000; Yan and Garey, 1997; Barone and Kennedy, 2000; Pereira et al., 2000; Hassiotis et al., 2005), no study has yet addressed the existence of any systematic variation in NADPH-d neuronal morphology across different primary areas. Based on the previously mentioned areal and morphological neuronal variations across brain regions, a re-examination of cerebral cortex architecture is stoutly recommend to get a better understanding of species specializations and evolutionary trends (Kaas, 2005; Krubitzer, 2009).

In the present work, we examined the morphological characteristics of layer IV NADPH-d neurons in three primary areas of the adult rat: primary somatosensory (S1), visual (V1), and auditory (A1) cortices. We performed our analysis in tangential sections because only in this way all cortical areas could be evaluated in a single section. We evaluated only layer IV neurons because a specific laminar position could be unambiguously attributed only to them, due to the intense neuropil staining characteristic of this layer in primary sensory areas. In rat S1, only labeled neurons located inside barrels were reconstructed to compare with those in A1 and V1. Septal cortex between barrels was excluded from this analysis because it displays functional and anatomical characteristics (Hayama and Ogawa, 1997; Kim and Ebner, 1999; Alloway, 2008) that might disqualify this region from being considered true primary sensory cortex (Kaas, 1983; Krubitzer and Hunt, 2007). Multivariate analysis of type I neurons accounted for different morphological parameters, and revealed that NADPH-d neurons were systematically different across different primary sensory areas. According to our results, neurons in S1 are more complex than those both in A1 and V1. This finding suggests the existence of a specialized and differentiated nitrergic cortical circuitry for each sensory modality.

EXPERIMENTAL PROCEDURES

Animals and experimental procedures

Seven adult male Wistar rats (*Rattus rattus*) (325±25 g), obtained from the Central Animal Facility of the Federal University of Pará (UFPA) were used. All efforts were made to avoid animal suffering and to reduce the number of specimens used. All experimental procedures were carried out strictly in accordance with the National Institute of Health Guide for the Care and Use of Laboratory Animals (NIH Publications No. 80–23), under license of the Ethics Committee on Experimental Animals of the UFPA.

The animals were deeply anesthetized with a mixture of ketamine chloridrate (2.5 mg/kg) and xylazine chloridrate (1 mg/kg) (i.p.) and perfused transcardially with 0.9% heparinized saline, followed by 4% paraformaldehyde (Sigma Company, St Louis, MO, USA) in 0.1 M phosphate buffer (PB), pH 7.4. After craniotomy, the brain was weighed, photographed, and the left hemisphere was separated from subcortical structures, flattened between two glass slides and immersed in 0.1 M PB overnight. The cortical sheet was then sliced tangentially at 100 μm with a vibratome (Pelco International, Series 1000, Ted Pella Inc., Redding, CA, USA). The resulting sections were washed three times in 0.1 M PB, pH 7.4 before histochemical processing. For NADPH-d histochemistry (*indirect* method) the sections were incubated in a solution containing 0.6% malic acid, 0.03% nitroblue tetrazolium, 1% dimethylsulfoxide, 0.03% manganese chloride, 0.5% β-NADP and 1.5–3% Triton X-100 in 0.1 M Tris buffer, pH 8.0 (Scherer-Singler et al., 1983). The reaction was monitored every 30 min to avoid overstaining and was interrupted by rinsing the sections in Tris buffer (pH 8.0). Sections were incubated in the same solution for all animals. The duration of the histochemical reaction ranged from 5 to 6 h. Finally, all sections were mounted onto gelatinized glass slides, air-dried overnight, dehydrated through a series of graded alcohols and coverslipped with Entellan (Merck, Germany). All reagents were purchased from the Sigma Company, USA.

Flattening of lissencephalic brains do not induce significant anamorphosis in the dorsolateral cortical surface (see Freire et al., 2010). In the present study, brain baseotomy was done in such way that the dorsolateral cortical surface becomes parallel to the stage of the sliding microtome and no discontinuity was observed in the flattened piece of cortex. For that reason no compensation was applied to the reconstructions.

Reconstruction procedures, qualitative and quantitative analysis

NADPH-d–labeled sections were qualitatively surveyed under light microscopy and images were obtained with a digital camera (CX9000, MBF Bioscience Inc., Williston, VT, USA) attached to an optical microscope (Nikon Eclipse 80i, Tokyo, Japan). Neurons from areas A1, S1, and V1 were also photographed to illustrate their morphologies. Only the contrast, and/or brightness of pictures were adjusted using Photoshop CS (Adobe Systems Inc., San José, CA, USA).

Three-dimensional (3D) reconstructions of NADPH-d type I neurons from areas S1, A1, and V1 (n=40 cells for each area) were performed with the *Neurolucida* system (MBF Bioscience Inc.) using a 60×-oil objective. Cells were selected for reconstruction depending on the integrity of the dendritic arborization in a single histological section. Only cells with unequivocally complete dendritic arborizations were included for analysis (more distal dendrites were typically thin, presenting a round tip). Cells whose dendrites seemed to be artificially cut or apparently not fully reacted were not included. Seven morphometric parameters were evaluated quantitatively in the reconstructed neurons: (1) area of dendritic arborization (defined by the polygon joining the outermost distal tips of the dendrites, in μm^2); (2) area of cell body, in μm^2; (3) number of dendritic branches per order; (4) dendritic length (length by dendrite order, and total length—sum of length of all dendrites); (5) branching complexity, using Sholl analysis (Sholl, 1953), with concentric circles spaced 25 μm from each other; (6) convex hull factor, a measure of dendritic coverage; and (7) fractal dimension (D). Fractal analysis was performed with the Scion Image software (Scion Corporation, Frederick, MD, USA), whereas the other measurements were obtained with the Neurolucida Explorer software package (MBF Bioscience Inc.).

For measurements of fractal dimension, we chose the dilation and the mass radius methods because they are the most sensitive methods (see Jelinek and Fernandez, 1998 for details). In brief, the dilation method determines D for each cell by overlaying the

original dendritic arborization with successively larger pixel arrays (dilation) and computing the relationship between the total dendritic length of each successive image with respect to the increasing width of the array (Jelinek and Fernandez, 1998). The mass-radius method, in turn, determines *D* from the relationship between the area of the image located within a sphere or circle of increasing radius covering the image, from the center (cell body) to the periphery (distal dendrites) of the image (Jelinek and Fernandez, 1998). To characterize distinct cell groups based on morphology, we performed a cluster analysis (Euclidean distance, complete linkage) (Schweitzer and Renehan, 1997) using area of dendritic arborization, cell body area, number of dendrites by order, convex hull factor, and fractal dimension as parameters. The resulting group distribution was submitted to a forward stepwise discriminant function analysis using the software Statistica 6.0 (StatSoft Inc., Tulsa, OK, USA) to determine which variables better discriminate the groups, a method successfully used to define clusters of neurons (Freire et al., 2010) and axon terminals (Rocha et al., 2007). In brief, we applied this multivariate statistical procedure to our sample to search for possible classes. The classes suggested by cluster analysis were assessed by a forward stepwise discriminant function analysis, a method used to determine which variables discriminate between two or more naturally occurring groups. The basic idea underlying this procedure is to determine whether groups differ with regard to the mean of a variable and then to use that variable to predict group membership. The software used in the present work (Statistica) performed comparisons between a matrix of total variances and covariances, as well as between matrices of pooled within-group variances and covariances. These matrices were compared via multivariate *F*-tests to determine whether or not there are any significant differences (with regard to all variables) between groups. In the forward stepwise discriminant function analysis, the computer program "builds" a model of discrimination step-by-step. In this model, at each step, the software reviews all variables and evaluates which one will contribute most to the discrimination between groups. We applied this procedure to morphological variables to determine which variables provided the best separation of classes suggested by cluster analysis. Additionally, arithmetic mean and standard deviation were calculated for the variables chosen as best predictors for groups.

In addition, a principal component analysis (PCA) was employed to decrease data dimensionality and allow intrinsic comparison among morphometric variables in the selected areas using Matlab software (the MathWorks Inc., Natick, MA, USA). The normalized data from PCA analysis were obtained by dividing the values of each group by their respective standard deviation.

For the statistical comparison amongst groups, we used both a non-parametric Kruskal–Wallis test and Pearson correlation followed by the Bonferroni post hoc test with significance level set at 95% (α=0.05). Average values were referred to as mean$\pm$ standard error of the mean (SEM). To avoid introduction of bias during the process of digitalization, only one person conducted all reconstructions. The data obtained were then analyzed independently by two different persons, one of who was unaware of the data's provenance (blind analysis). Afterward, both analyses were compared to check for differences.

Reconstructions of neurons evaluated in the present work will be publicly available for download at http://neuromorpho.org, a free online repository service for digitally reconstructed neuronal structures (Ascoli et al., 2007).

RESULTS

General pattern of NADPH-d reactivity

The tangential distribution of NADPH-d–reactive neuropil across layer IV allowed the identification of cortical areas A1, S1, and V1 (Fig. 1A). The boundaries and relative location of these areas were congruent with previously published reports (Woolsey, 1967; Wallace, 1987; Remple et al., 2003).

Four distinct fields were identified in S1, corresponding to the head, forelimb, hind limb, and trunk representations. The head representation could be further divided into subfields representing the whisker pad (posteromedial barrel subfield—PMBSF) and the upper and lower lips (Fig. 1A). Representations of hind limb and trunk lie more medially while face and head are located more laterally, in an upside-down orientation (Santiago et al., 2007). All representations (except for the trunk) had an intrinsic modular organization composed of barrels and septa, as previously revealed by histological (Welker and Woolsey, 1974) and histochemical methods (Franca and Volchan, 1995).

The auditory cortex was identified as an oval-shaped region located laterally from the head representation in S1, whereas the primary visual area corresponded to a "v-shaped" region located at the posterior pole of the cortex (Fig. 1A).

Qualitative aspects and quantitative analysis of NADPH-d type I neuronal morphology

Two types of NADPH-d-reactive neurons were readily identified in the rat's brain: type I and type II cells (Lüth et al., 1994). Both groups correspond to non-pyramidal neurons with distinct labeling patterns (Fig. 2A). Briefly, type II neurons had a small cell body and a faintly labeled or even absent dendritic arborization. So it was rather difficult to classify them due to their diminished body size and the absence of most dendritic detail (see Fig. 2A). Due to the lack of morphological detail as revealed by NADPH-d, type II cells were not included in our analysis. Conversely, type I cells were intensely labeled with sharp tapering dendrites (Figs. 1B and 2). The overall morphology of type I neurons was quite diverse, including multipolar, stellate, and bipolar cells (Fig. 2B–D).

Qualitative evaluation of type I NADPH-d neurons morphology in the different hemispheres analyzed did not point to any apparent differences inside a given cortical area. For instance, aspects like dendritic size, cell body location, labeling intensity, dendritic orientation, and distribution along the cortical area did not seem to differ. We thus assumed that any type I neuron would be an equally good representative for the quantitative analysis, provided its dendritic arbor is complete.

The morphology of type I neurons was then quantified using seven morphometric parameters (see Experimental procedures). There was no significant difference in cell body areas among primary sensory regions (S1: 255.34$\pm$5.54 μm^2, A1: 271.54$\pm$13.03 μm^2, V1: 267.88$\pm$8.09 μm^2) (Fig. 3A). Conversely, dendritic field areas were significantly different among areas: neurons in S1 had larger dendritic fields than both A1 and V1 cells (S1: 35.31$\pm$0.94$\times 10^3$ μm^2; A1: 29.70$\pm$1.09$\times 10^3$ μm^2; V1: 24.34$\pm$0.97$\times 10^3$ μm^2) (Fig. 3B). The same occurred with the number of dendrites by order: neurons located in V1 had fewer ramifications than those in A1 and especially than in

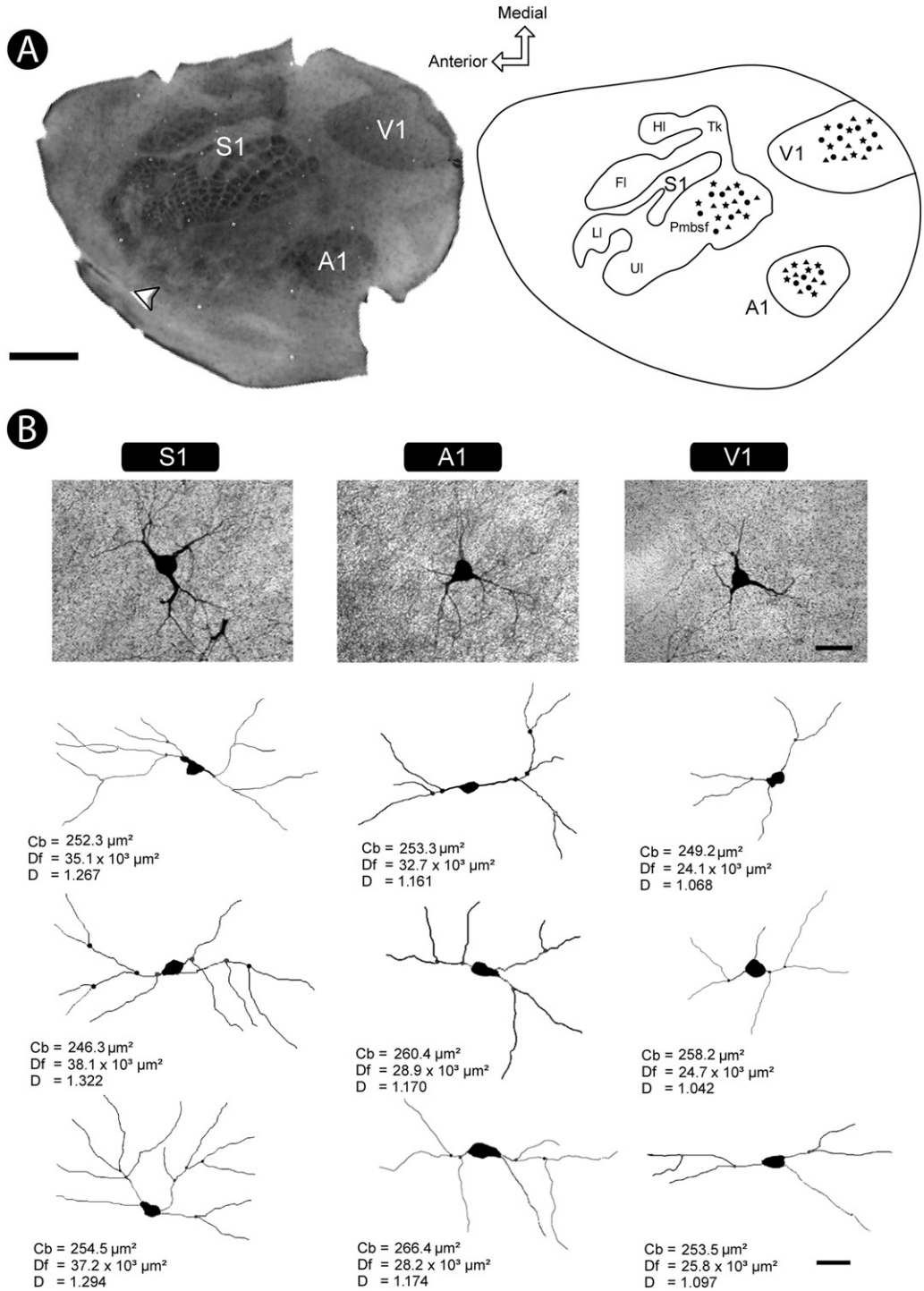

Fig. 1. NADPH diaphorase-reactive neuropil and NADPH diaphorase neurons across primary sensory areas. (A) Left side: tangential section across layer IV reacted for NADPH-d histochemistry. Neuropil reactivity allows identification of primary auditory (A1), somatosensory (S1), and visual (V1) areas. The white arrowhead points to the rhinal fissure. (A) Right side: reconstruction of the flattened cortex showing the limits of primary areas, including S1 subdivisions, and the estimated location of NADPH-d neurons reconstructed in A1, S1, and V1 from three different cases, represented by distinct symbols (circles, triangles, and stars—each symbol representing cell from a different animal). (B) Examples of NADPH-d neurons from the three primary areas analyzed. Each column corresponds to the cortical area depicted in the photomicrograph. Three morphometric parameters are illustrated for every reconstructed neuron: cell body area (Cb), dendritic field area (Df), and fractal dimension (D). Neurons found in S1 display a more complex dendritic morphology than those located in A1 and V1. Neurons in V1 present the least complex dendritic morphology. The values of Cb, Df and D reported in the bottom of the reconstructions correspond to values from the individual cells illustrated. Scale bars: 1 mm (A); 30 μm (B). Legends: PMBSF: posteromedial barrel subfield; Ll: lower lip; Ul: upper lip; fl.: forelimb; Hl: hind limb; Tk: trunk.

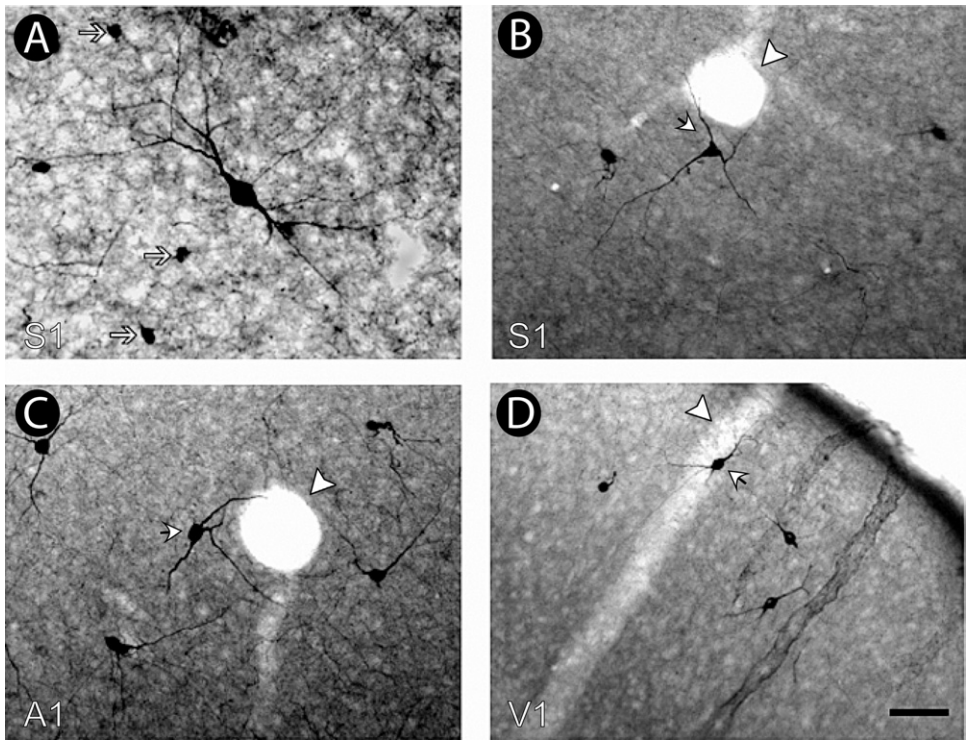

Fig. 2. Morphology of NADPH-d cell types I and II. (A) Type I neurons have considerably larger cell bodies, more exuberant dendritic fields and stain more heavily than type II neurons (arrows). (B–D) The overall morphology of type I neurons was quite diverse, including stellate (B), multipolar (C), and bipolar (D) (arrows). Arrowheads: blood vessels. Scale bars: 50 μm (A); 100 μm (B–D).

S1. The maximum ramification occurred in the second order dendrites for all groups (Fig. 3C). In all groups, second order dendrites were the longest (Fig. 3D). In addition, neurons in S1 had larger total dendritic length than A1 and V1 (S1: 951.80±26.61 μm; A1: 754.31±23.84 μm; V1: 630.45±19.09 μm) (Fig. 3E). Sholl analysis revealed that NADPH-d neurons in V1 were less ramified than those in A1. S1 cells had the most complex dendritic arborization, having more ramifications than both A1 and V1, mainly in a distance between 75 and 125 μm from the cell body (intermediary dendrites) (Fig. 3F).

The higher morphological complexity of S1 interneurons, as compared to those of V1 and A1, was further corroborated by the fractal (dilation and mass radius methods) and convex hull analysis. Both fractal measurements pointed out that S1 neurons have more complex dendritic trees than both A1 and V1 neurons, with the latter having the simplest dendritic trees (S1: dilation: 1.385±0.020; mass radius: 1.412±0.022; A1: dilation: 1.307±0.038; mass radius: 1.346±0.018; V1: dilation: 1.216±0.028; mass radius: 1.267±0.014) (Fig. 4A, B). The convex hull analysis corroborated this tendency: V1 interneurons were significantly less complex than those in both A1 and S1. Values for A1 cells were intermediary between S1 and V1 (V1: 1.348±0.041; A1: 1.477±0.047; S1: 1.543±0.053; $P<0.01$) (Fig. 4C). Performing a statistical comparison with "*n*" as the number of animals, the statistical results were similar to those obtained evaluating "individual neurons" (Table 1).

According to the analysis of variance, dendritic complexity (measured by the dendritic field area and fractal dimension) explains most morphologic variance within sensory areas (Fig. 5A). In every sensory area, correlation analysis between pairwise combinations of morphometric parameters showed a positive and significant correlation between fractal dimension and dendritic field area (S1: $r=0.7651$, $P=0.020532$; A1: $r=0.57222$, $P=0.04958$; V1: $r=0.66858$, $P=0.043786$) (Fig. 5B). Fig. 6A shows the explained variances for the components of each neuronal attribute (area of cell body, dendritic field area and fractal dimension). Areas V1, A1, and S1 were grouped together to see how they covariate according to each attribute. According to PCA analysis, fractal dimension exhibits the maximum variance in the first component, suggesting that this attribute is most correlated along the three areas. Fig. 6B shows the explained variances for each component considering each cortical area (V1, A1, and S1). The neuronal attributes were grouped to verify how they covariate in each area. In this case, the information is more uniformly distributed, with no evident tendency toward any attribute's direction. Fig. 6C shows linear regression crossing for each first component of every cortical area, by extracting the covariance of neuronal features.

Cluster analysis of neuronal morphological data

Fig. 7 shows the dendrograms obtained from cluster analysis performed on data from all 120 neurons in our sample.

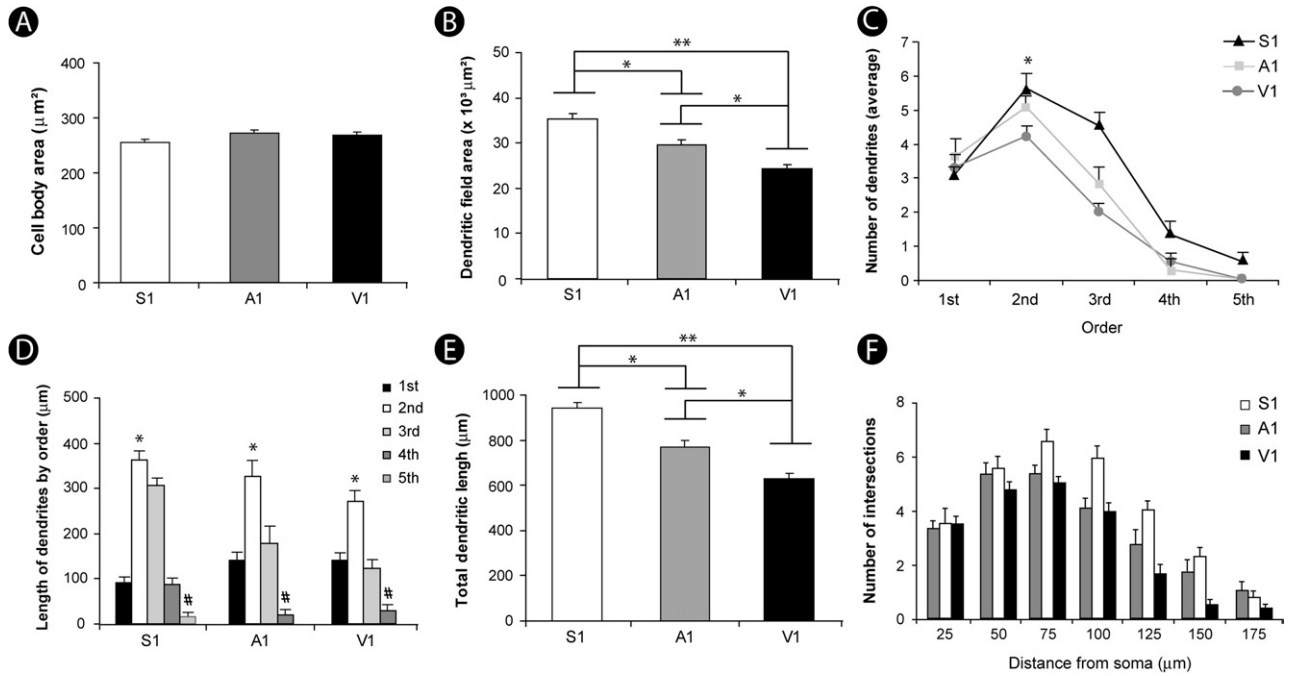

Fig. 3. Morphometric analysis of NADPH-d type I neurons in primary sensory areas S1, A1, and V1. (A) Cell body areas are not significantly distinct across cortical areas ($P>0.05$). (B) Dendritic field areas are significantly different, with neurons found in area S1 having the largest dendritic coverage (* $P<0.05$ and ** $P<0.01$, respectively; Kruskal–Wallis Bonferroni post hoc test). (C) In all three cortical areas, second order dendrites are more numerous (* $P<0.05$). (D) Second order dendrites are longer than first, third, fourth, and fifth order dendrites in all three areas (* $P<0.05$). More distal dendrites are significantly shorter as compared with the proximal and intermediate ones (# $P<0.01$). (E) Neurons of S1 had the longest dendrites, as compared with A1 (* $P<0.05$) and V1 (** $P<0.01$). (F) Sholl analysis revealed that NADPH-d neurons in S1 have a more exuberant dendritic arborization, followed by A1 and V1 cells.

By using a multivariate analysis, we were able to separate three groups of cells, each one in a distinct cortical region. Particularly, when comparing V1 and S1, 15% of the neurons from the former clustered with the latter, whereas 17% of S1 neurons clustered with the V1 group (Fig. 7A). When neurons from S1 and A1 are compared, only 6% neurons from A1 clustered with S1, whereas 18% of the neurons from S1 were also found in the A1 cluster (Fig. 7B). On the other hand, the A1×V1 comparison produced clusters that were the least segregated, with 28% V1 neurons clustering with the A1 group, whereas 35% of A1 neurons clustered with the V1 group (Fig. 7C). The higher the values observed in y-axis of dendrograms the more distantly related the clusters are (S1×V1, Fig. 7A, A1×V1, Fig. 7C). Conversely, S1×A1 clusters are closest to each other, as attested by the lesser value of Euclidean distance between them (Fig. 7B).

The discriminant analysis indicated that the four major variables contributing to cluster separation were dendritic field area, total length of dendrites, fractal dimension, and convex hull number (Table 2). As mentioned previously, discriminant analysis showed that S1 neurons had higher dendritic complexity than cells found in both V1 and A1 ($P<0.05$). V1 neurons were always less complex than those found in both S1 and A1 ($P<0.05$). Cell body size did not contribute significantly to group formation, according to discriminant analysis ($P>0.05$).

DISCUSSION

We evaluated how the morphology of interneurons stained with NADPH-d varies across the cortical primary sensory areas of the rat. Our principal result was that neurons in S1 have a much more complex dendritic arborization than those located in both A1 and V1, with V1 neurons having the simplest dendritic arbors. These findings were corroborated by a statistical analysis of quantitative morphological data, which showed that neurons in our sample clustered in three groups with distinct morphologies. We discuss the significance of these findings below.

Neuropil reactivity and types of NADPH-d neurons

The general pattern of NADPH-d–reactive neuropil allowed a clear distinction of areal borders and the relative location of cortical areas S1, A1, and V1. The results reported here for the rat corroborate and extend previous descriptions of NADPH-d as an outstanding marker of primary areas in distantly related species (Franca et al., 1997, 2000; Freire et al., 2010). In addition, the boundaries of primary sensory cortical areas defined by NADPH-d–reactive neuropil are markedly similar to those defined by electrophysiology and other histochemical markers in the rat, such as cytochrome oxidase (CO) and succinate dehydrogenase (SDH) (Woolsey, 1967; Wallace, 1987; Remple et al., 2003). Because nitric oxide acts as a retrograde messenger that increases the activity of presynaptic

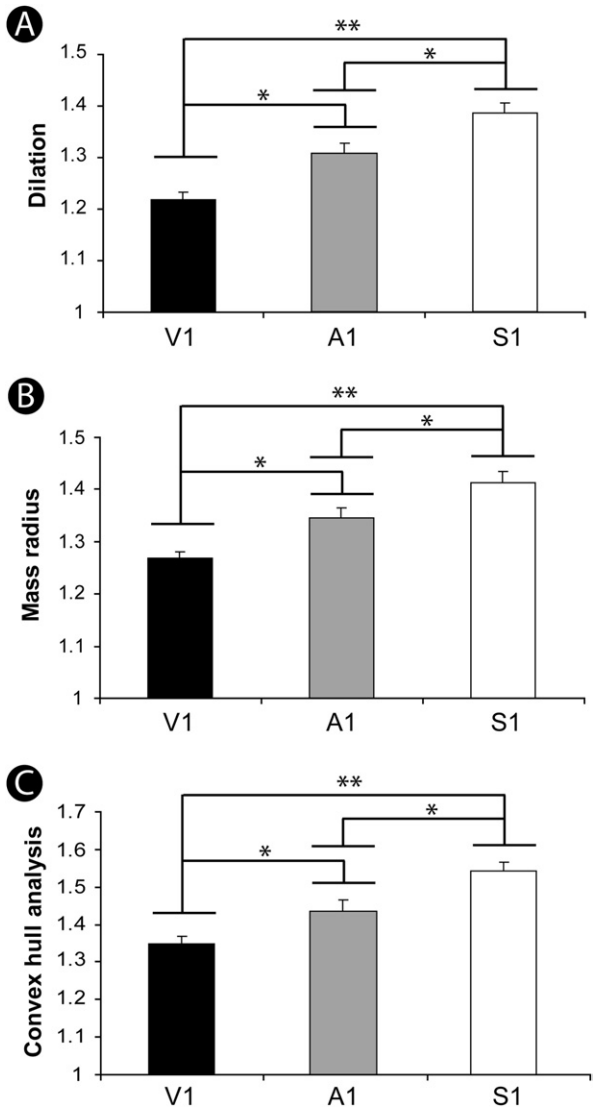

Fig. 4. Morphological complexity of NADPH-d type I neurons throughout primary sensory areas. (A and B) NADPH-d neurons in S1 presented fractal dimension numbers that are significantly higher than of the ones for NADPH-d neurons in both A1 and V1 (A: measurement by the dilation method; B: measurement by the mass radius method). This result is corroborated by the convex hull analysis (C) (* $P<0.05$ and ** $P<0.01$, respectively; Kruskal–Wallis Bonferroni post hoc test).

terminals (Garthwaite, 2008), the correspondence between the histochemical labeling of NADPH-d and CO in primary areas can be explained by the higher energetic metabolism necessary to maintain neural activity in these cortices (Wong-Riley et al., 1998).

We identified two morphologically distinct groups of non-pyramidal NADPH-d–reactive interneurons across primary sensory areas of the rat, one with large cell bodies and a highly ramified and reactive dendritic arborization (type I), whereas the other is characterized by small and faintly stained cell bodies, without reactive dendrites (type II). Although the presence of the former group has been confirmed in every mammalian species studied so far (DeFelipe, 1993b; Xiao et al., 1996; Franca et al., 1997, 2000; Barone and Kennedy, 2000; Hassiotis et al., 2005; Freire et al., 2008, 2011), the universality of type II neurons is still a matter of some controversy because an early study claimed it could not be found in rodents (Yan and Garey, 1997). However, our group have already provided unequivocal evidence for the presence of type II NADPH-d–reactive cells in the rodent brain (Freire et al., 2004, 2005), suggesting that previous failure in detecting these cells might be due to methodological issues. Knowing that more intense tissue fixation can decrease NADPH-d histochemical activity (Spessert and Layes, 1994), we suggested that detection of NADPH-d type II cells would be impaired by intense fixation, either because type II cells express less enzyme than type I neurons or because they express an enzyme subtype that is more sensitive to fixatives, or both.

Morphometric differences as an evidence of the cortical heterogeneity

There are two hypotheses to explain the microstructure of the mammalian cerebral cortex. The first one posits that the neocortex is composed of repeated columns of cells that form a canonical microcircuit (Douglas et al., 1989; Mountcastle, 1997; Binzegger et al., 2004). This hypothesis is based in electrophysiological evidence (such as topographic maps and receptive field properties) and the stereotyped laminar and columnar input-output organization of the cortex (Kaas, 1987; Schubert et al., 2007). The other, conversely, states that neuronal structure and patterns of connectivity vary widely throughout the cortex and that there is no such thing as a canonical circuit (Nelson, 2002; Elston, 2003; Horton and Adams, 2005). If we assume that the former hypothesis is correct, regional differences in primary cortical function (hearing, vision, and somatosensory processing) might be attributed essentially to the source of their inputs. Nevertheless, if we accept the latter as correct, as described to pyramidal cells (Benavides-Piccione et al., 2006), probably the differences in the

Table 1. Statistical comparison of morphometric variables across primary areas considering "*n*" as number of animals

Variable	Cortical area			*P*
Cell body area (μm^2)	S1: 258.19±7.96#	A1: 273.94±4.26#	V1: 262.9±±19.63#	>0.05#
Dendritic field area ($\times 10^3$ μm^2)	S1: 35.77±1.12**	A1: 30.21±1.11**	V1: 24.7±1.06**	<0.05*
Total dendritic length (μm)	S1: 961.27±32.47 **	A1: 742.52±27.57 **	V1: 634.29±28.43 **	<0.01**
Fractal dimension (dilation)	S1: 1.544±0.038**	A1: 1.424±0.059*	V1: 1.292±0.047**	
Fractal dimension (mass radius)	S1: 1.596±0.074**	A1: 1.484±0.053*	V1: 1.376±0.049**	
Convex hull	S1: 1.477±0.025*	A1: 1.346±0.018*	V1: 1.247±0.034*	

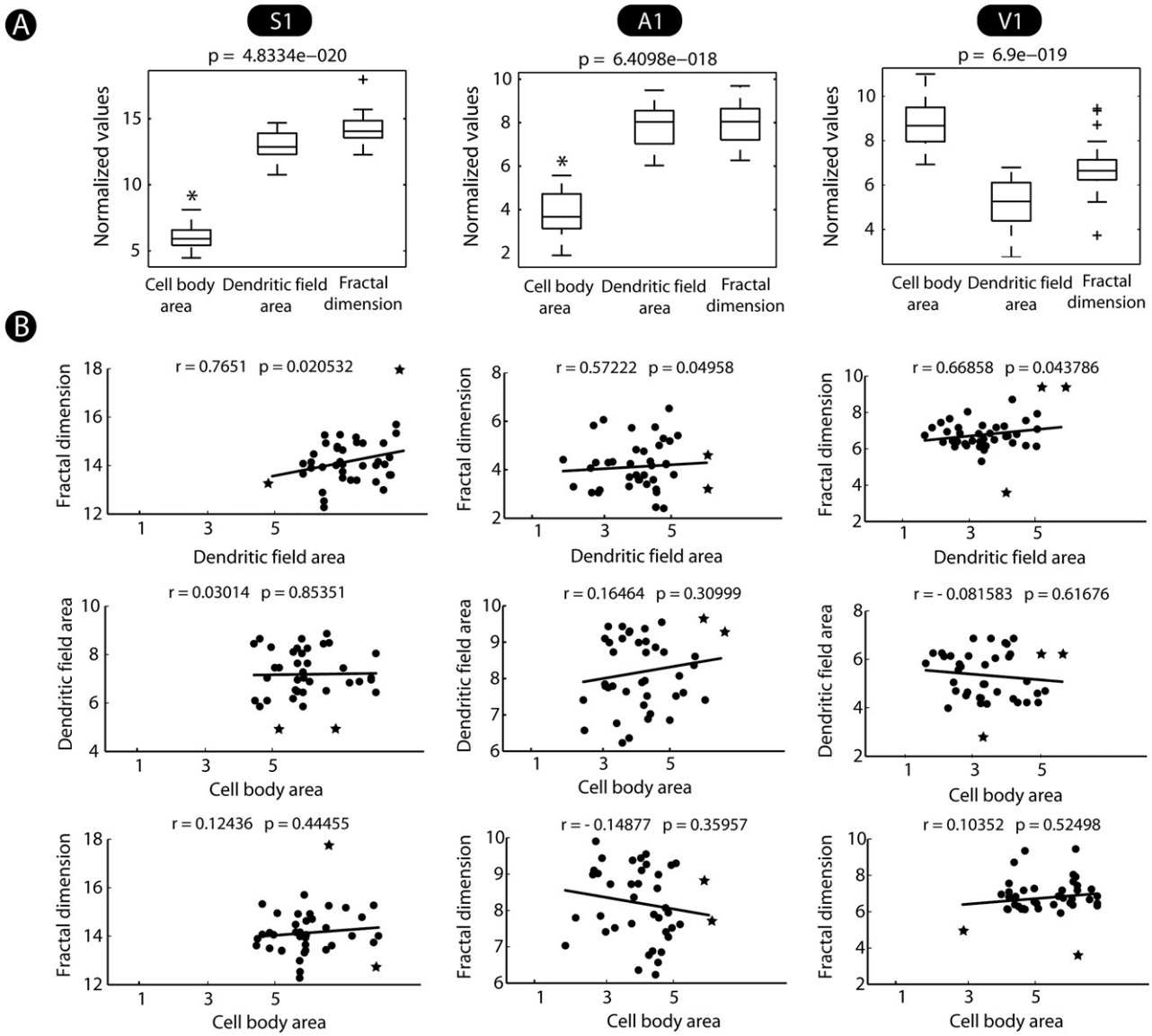

Fig. 5. Analysis of variance and linear regression among morphometric data. (A) According to analysis of variance, dendritic complexity (measured both by the dendritic field area and fractal dimension) explains most morphological variance within sensory areas, except in V1 (*$P<0.05$, Kruskal–Wallis Bonferroni post hoc test). (B) Comparison among morphometric parameters showed a positive and significant correlation between fractal dimension and dendritic field area (Pearson correlation). The normalized data were obtained by dividing the values of each group by their respective standard deviation.

circuitry should not to be restricted to a specific type of neuronal group. Accordingly, our data are more in agreement with the latter proposal: the morphology of NADPH-d type I neurons differ significantly among the rat's primary sensory areas. Both the cellular distribution and morphological heterogeneity of NADPH-d neurons actually seem at odds with the existence of repeated copies of a canonical circuit across the cerebral cortex (Douglas and Martin, 2004). We had already demonstrated that the distribution of these cells is not uniform in rat's brain: the density of NADPH-d neurons is higher in somatosensory than in the visual cortex (Franca et al., 2000). This seems to be a general rule that applies not only to the rat but also to monkeys and even to non-eutherian mammals like the opossum (Franca et al., 2000).

Although these data are compelling arguments against the canonical microcircuit proposal, we cannot entirely exclude the possibility that a repetitive cortical circuit appeared early in evolution of the neocortex and that, later, novel neuronal populations were added to this basic circuit. As the neocortical sheet evolved through phylogeny and new cortical areas appeared by duplication (Krubitzer, 1995), new circuit elements could have been added in some cortical areas but not in others. Distribution and morphology of these new populations would not obey the original ontogenetic rules that defined cellular distribution

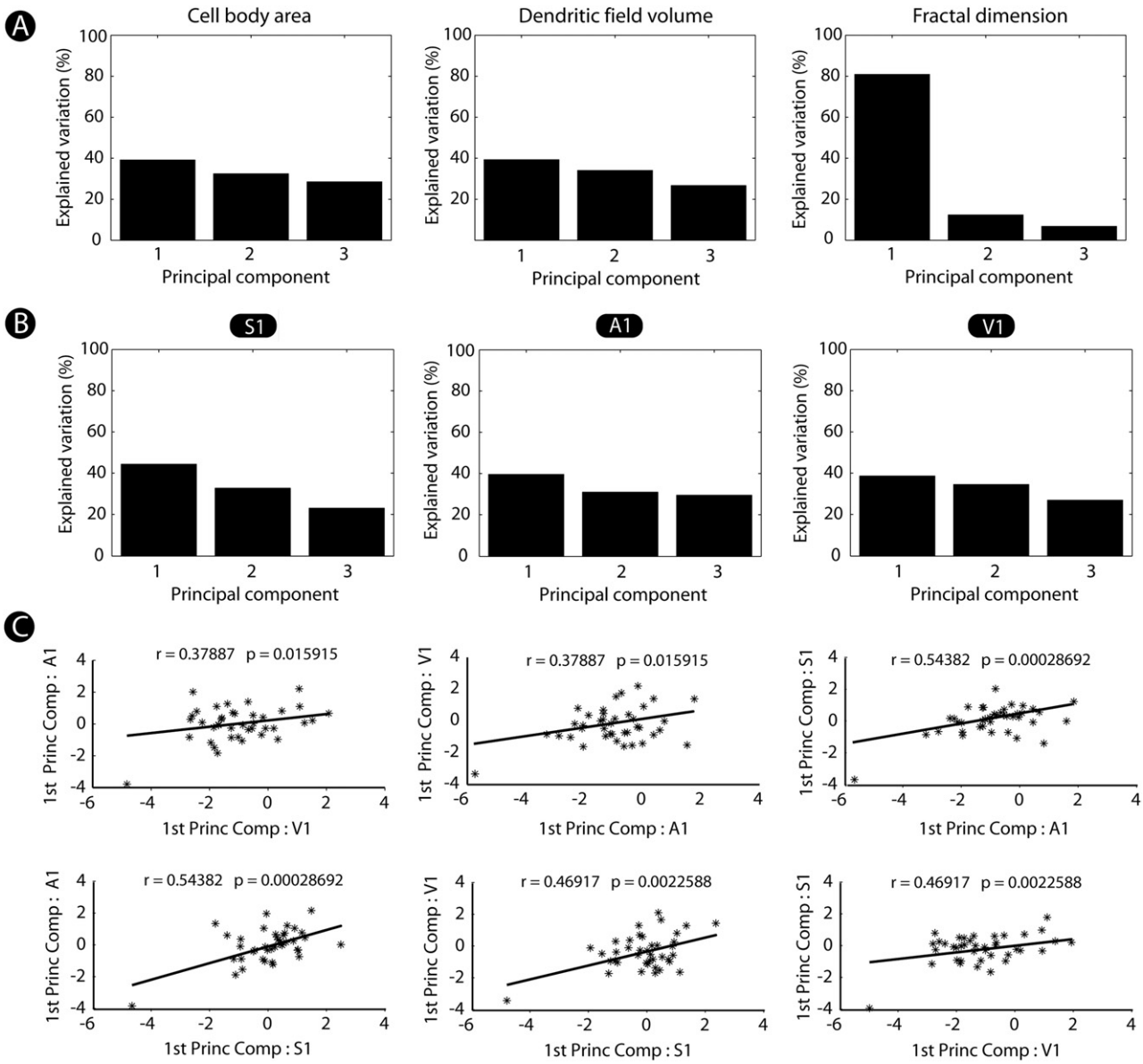

Fig. 6. Principal component analysis (PCA) of neuronal attributes. Fig. 6A shows the explained variances for the components of each neuronal attribute: area of cell body, dendritic field area, and fractal dimension. Areas V1, A1, and S1 were grouped together to see how they covariate according to each attribute. Fractal dimension exhibits the maximum variance in the first component, suggesting this attribute is most correlated along the three areas. Fig 6B shows the explained variances for each component considering each cortical area (V1, A1, and S1). The neuronal attributes were grouped to verify how they covariate in each area. In this case, the information is more uniformly distributed, with no evident tendency toward any attribute's direction. Fig. 6C shows linear regression crossing for each first component of every cortical area, by extracting the covariance of neuronal features.

and morphology of the primordial cortical circuit elements. Because of the characteristic heterogeneous spatial distribution and morphology of NADPH-d neurons along the cortical sheet (Franca et al., 2000; Freire et al., 2010) we do rule out the possibility that this subpopulation of inhibitory neurons is part of a repetitive microcircuit as proposed by Douglas and Martin (2004). Because GABAergic inhibitory interneurons should definitively be part of a putative canonical microcircuit, further studies about the spatial distribution of other subcategories of inhibitory interneurons should be performed to clarify this issue. In addition, the quantification of NADPH-d neuronal morphology in non-primary/association areas also can undeniably provide a more complete notion of cortical differences in the inhibitory circuitry.

Here we characterize a significant difference in the ramification of dendritic trees of NADPH-d type I cells across primary areas in the rat: neurons become increasingly larger and progressively more branched in these areas along the caudorostral axis. For instance, cells in S1 were, on average, about 31% larger and 30% more branched than those in V1. These morphological differ-

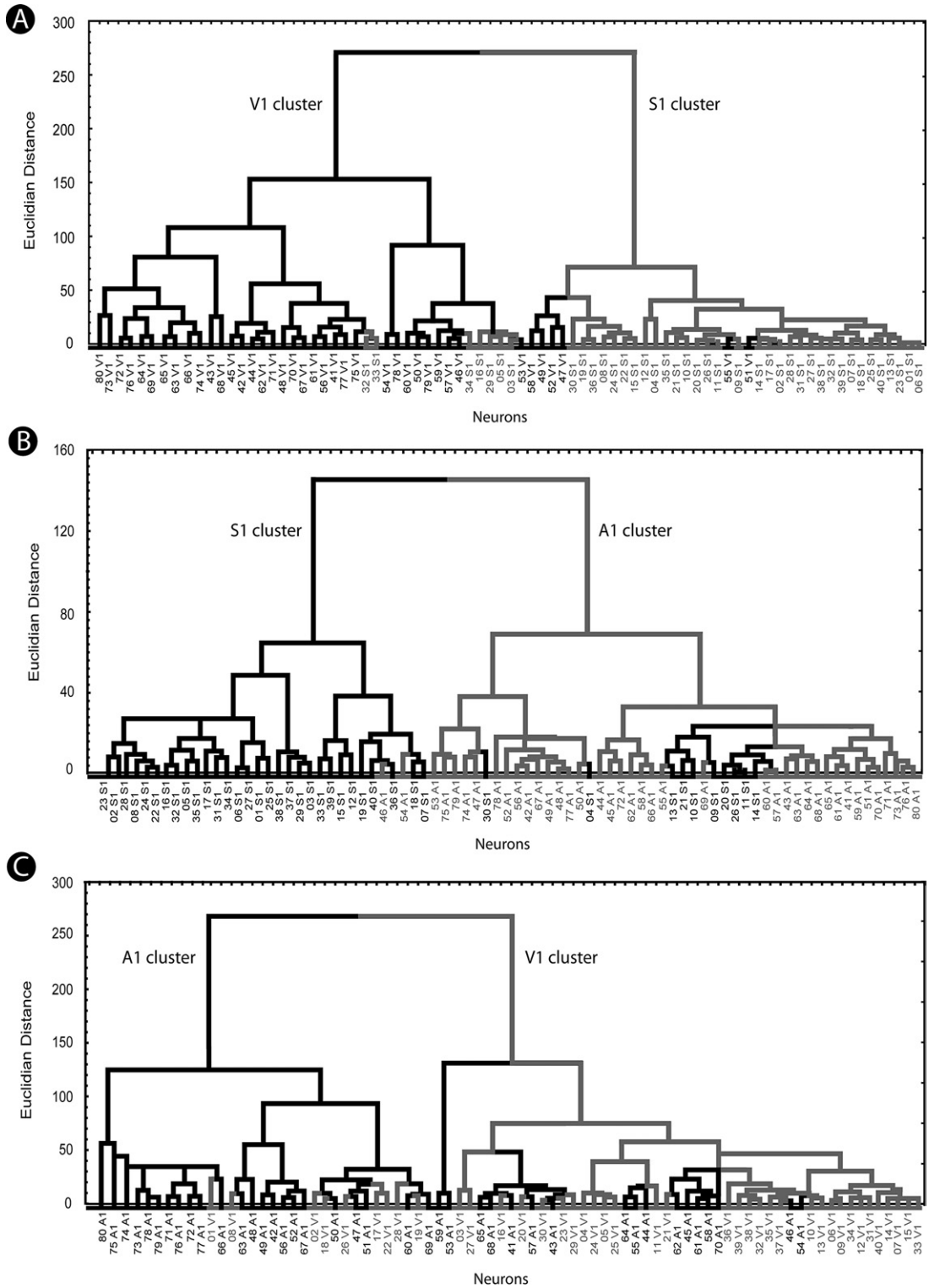

Fig. 7. Dendrograms from the resulting cluster analysis (Euclidian distance, complete linkage method). Numbers and letters at the bottom of each tree branch denote the identification number of a single reconstructed NADPH-d neuron and the cortical area to which it belongs. To better evaluate the clustering, the color of branches, letters, and numbers that refer to individual neurons are either gray or black, corresponding to one of the two different cortical areas compared in each dendrogram (i.e. V1 vs. S1, S1 vs. A1, or V1 vs. A1). Neurons found in S1 and V1 tended to be located at the extremes of this distribution (A). A1 neurons, conversely, tended to be grouped in the center, when compared with S1 cells (B). Neurons of A1 and V1 were found to be less segregated from each other (C).

Table 2. Summary of discriminant function analysis for all variables evaluated

Variable	Cortical area			*P*
Cell body area	S1 vs. A1#	S1 vs. V1#	A1 vs. V1#	>0.05#
Dendritic field area	S1 vs. A1*	S1 vs. V1**	A1 vs. V1*	<0.05*
Number of dendrites by order	S1 vs. A1*	S1 vs. V1**	A1 vs. V1*	<0.01**
Dendritic length	S1 vs. A1*	S1 vs. V1**	A1 vs. V1*	
Branching complexity (Sholl analysis)	S1 vs. A1*	S1 vs. V1*	A1 vs. V1*	
Fractal dimension—dilation	S1 vs. A1*	S1 vs. V1**	A1 vs. V1*	
Fractal dimension—mass radius	S1 vs. A1*	S1 vs. V1**	A1 vs. V1*	
Convex hull	S1 vs. A1*	S1 vs. V1**	A1 vs. V1*	

ences of NADPH-d neurons across the rat's brain appear to point out a wide-ranging feature in the rodent brain, because these cells become progressively more complex throughout the visual areas of the agouti, a typical Amazonian rodent (Freire et al., 2010). How would these specializations in neuronal morphology influence cortical processing? Small rodents are usually nocturnal species, possessing very specialized tactile organs, the facial whiskers, which help them navigate in darkness (Vasconcelos et al., 2011). A thick bundle of low-threshold sensory axons connects the whiskers through intervening relay nuclei to the barrel field in S1. Vision and audition, by contrast, are relatively less developed in rats (Hoeffding and Feldman, 1988). Thus, the relatively more complex pattern of dendritic arborization observed in S1 compared with V1 could reflect the prominence of tactile-mediated behavior in the rat. It is conceivable that area-specific developmental factors that either restrict or stimulate the number of NADPH-d neurons are also acting to inhibit or stimulate their dendritic development. Moreover, these structural differences could reflect a modality-driven specialization in the processing of sensory information (Nelson, 2002). The heterogeneous morphology of the dendritic field in cortical interneurons, for instance, could mean a difference in their capacity for synaptic integration because dendritic coverage is directly related to the amount of synaptic contacts a cell can receive. So, neurons possessing a smaller dendritic arbor cover a small cortical area and potentially establish fewer synaptic contacts than more ramified cells, given that differences in microcircuitry are likely to be instrumental in determining neuronal function throughout the cortex.

Additionally, NADPH-d–reactive cells are a source of NO. This substance is implicated in several important physiological and pathological functions in the brain, including plasticity, neuroprotection, and neurotoxicity (Calabrese et al., 2007; Freire et al., 2009; Guimarães et al., 2009; Steinert et al., 2010; Pietrelli et al., 2011). In particular, NO seems to be directly involved in the coupling of cerebral blood flow with demands of brain activity (Iadecola et al., 1993; Schottler et al., 1996; Estrada and DeFelipe, 1998; Govsa and Kayalioglu, 1999). Its association with NPY, a powerful vasoconstrictor (Vincent et al., 1983), raises interesting possibilities about their combination and the fine regulation of blood flow in specific cortical areas throughout functional activity. While NO release by the cell body and dendrites produces local vasodilation, this effect may be restricted distally by the vasoconstrictive action of NPY released by the neuron axon. By this mechanism, the vasodilation would be circumscribed to the area around the neuronal soma and dendrites (Estrada and DeFelipe, 1998). This may have important implications for the physiological role of type I NADPH-d neurons in rat barrel cortex, given that as more ramified a cell is the greater is the influence it can exert in a specific cortical area. Cells inside barrel hollows are thus in a good position to control most efficiently blood flow toward the center of the barrels, a highly metabolic and vascularized region (Woolsey et al., 1996). Additional work is nonetheless needed to evaluate whether NADPH-d neurons inside barrels display different morphological features as compared with those in septal cortex of the rat.

Methodological considerations

In the present work, we reconstructed only NADPH-d type I cells, since this subgroup possesses well-labeled and clear-cut dendritic arborizations. Type II neurons, conversely, presents small sized cell bodies and weakly stained or even non-reactive dendritic trees that prevents their reconstruction, unless they are marked with intracellular injected labels like Lucifer Yellow (Kubota et al., 2011). On the same token, there is no intrinsic guarantee that based on the NADPH-d label only, the dendritic arbors of the type I cells selected here for reconstruction are complete. Nonetheless, we can rely on NADPH-d as a marker for the presence of constitutive nitric oxide activity in these cells. Thus, it remains to be clarified by further studies using intracellular labeling of type I NADPH-d neurons whether nitric oxide synthase activity is in fact widespread throughout the whole dendritic arbor or whether it is compartmentalized along the cell.

Additionally, despite the fact that we tried not to reconstruct neurons with sectioned dendrites (i.e. dendrites without a tapering profile), it is likely that in some of them part of the dendritic tree was missing, especially in those vertically oriented neurons. This is because type I neuron dendrites can extend over 175 μm (Fig. 3F), at least in the horizontal/tangential plane and our reconstructions were performed in 100-μm-thick sections. Nevertheless, despite the possibility of such a bias, this methodological issue would not explain the morphological differences we found when neurons from different cortical areas are compared, unless if type I cells in V1 were predominantly vertically oriented as compared with those in S1 and A1, which was not the case. Further analysis of the spatial distribution of the dendritic arborization in non-tangential planes of section is thus needed to elucidate if dendritic arbor orientation differs in different cortical areas.

In the present work, we chose to separate the cortical sheet from other subcortical structures and then flatten the tissue between two glass slides. Tissue flattening is especially useful to analyze anatomical data obtained from highly convoluted brains (Gharbawie et al., 2011). Taking advantage of the two-dimensional sheet topology of the cortical surface, cortical tissue flattening facilitates the collection and interpretation of anatomical data by optimizing the plane of section. This occurs because the curved cortical surface is made parallel to the cutting knife by the flattening process. This procedure potentially brings to single-section profiles that would otherwise be dispersed in different transverse histological sections. Additionally, flattening procedures associated with a tangential plan of section is also advantageous because it allows a global view of the cortical areas of interest in only one section (Rocha et al., 2007; Freire et al., 2010) that would not be feasible using other plans of sectioning. With such global appreciation of areal boundaries, we ensured that the neurons selected for reconstruction were unequivocally located in cortical areas of interest (S1, A1, or V1), thus preventing that cells located in adjacent areas were incorrectly selected. Finally, although it is mathematically impossible to flatten curved surfaces without metric and area distortion (Hurdal and Stephenson, 2009), it is worth noting that in lissencephalic brains morphological distortion caused by flattening should be minimal not only because the angle that defines the curve of the cortical sheet is wide (around 120 degrees in gross estimation), but also because the horizontal range of NADPH-d dendritic arbors reconstructed in the present work is very short when compared with the total range of the flattened cortical sheet.

There are several methodological issues that have to be taken into consideration related to tissue shrinkage and other structural modifications introduced by tissue processing. For instance, due to mechanical factors associated with the sectioning apparatus (a vibratome, in our case), the section surface can be uneven and asymmetrical. As for the *z* dimension (i.e. depth), actual thickness of histological sections tends to be much smaller than that set for microtomy in the vibratome. Thus, estimates of modifications in the *x*/*y* dimensions during tissue processing cannot be linearly extrapolated to the *z* dimension. These are methodological constraints that are difficult to overcome. However, it is important to note that an indicative of a severe shrinkage in *z*-axis is the curling of dendrites, signifying that individual processes did not shrink at the same rate as the slice in which they are located (Jaeger, 2000). This pattern was not observed in the reconstructed cells of our study (see Fig. 1).

CONCLUSION

It is possible to group, according to their morphological characteristics, NADPH-d neurons in discrete clusters corresponding to different primary sensory areas of the rat, most likely reflecting an intrinsic specialization of the inhibitory circuitry throughout the cerebral cortex. This finding is in agreement with the hypothesis that neuronal structure vary widely across the brain. Cells increased systematically in both size and branching complexity with a caudorostral progression from V1 to A1 and S1. Given that the relatively more complex pattern of dendritic arborization was observed in S1, this specialization may reflect the prominence of tactile-mediated behavior in the rat. More comparative studies evaluating other groups of inhibitory neurons and also in non-primary/associative areas will be useful to provide a comprehensive picture of the specializations in the inhibitory circuitry across rodent sensory areas.

Acknowledgments—We would like to thank two anonymous referees for their helpful comments and propositions. Work supported by grants from Financiadora de Estudos e Projetos (FINEP - Rede Instituto Brasileiro de Neurociência (IBN Net), FINEP Ref. 4191/05—Encomenda Ação Transversal, Proc. no. 01.06.0842–00), Programa de Apoio a Núcleos de Excelência (PRONEX-MCT) and FAPERJ—Brazil. A.P., J.G.F. and C.W.P.D. are CNPq research fellows.

Author contributions

MAMF, JGF and AP conceived and designed the experiments; MAMF performed the experiments; MAMF and JF analyzed the data; MAMF, JF and JGF designed and organized the illustrations; AP, JF and CWPD contributed with reagents/materials/analysis tools; All the authors contributed to the writing of the article.

REFERENCES

Alloway KD (2008) Information processing streams in rodent barrel cortex: the differential functions of barrel and septal circuits. Cereb Cortex 18:979–989.

Aoki C, Pickel VM (1990) Neuropeptide Y in cortex and striatum. Ultrastructural distribution and coexistence with classical neurotransmitters and neuropeptides. Ann N Y Acad Sci 611:186–205.

Ascoli GA, Donohue DE, Halavi M (2007) NeuroMorpho. Org: a central resource for neuronal morphologies. J Neurosci 27:9247–9251.

Barone P, Kennedy H (2000) Non-uniformity of neocortex: areal heterogeneity of NADPH-diaphorase reactive neurons in adult macaque monkeys. Cereb Cortex 10:160–174.

Benavides-Piccione R, Hamzei-Sichani F, Ballesteros-Yáñez I, DeFelipe J, Yuste R (2006) Dendritic size of pyramidal neurons differs among mouse cortical regions. Cereb Cortex 16:990–1001.

Bidmon HJ, Wu J, Gödecke A, Schleicher A, Mayer B, Zilles K (1997) Nitric oxide synthase-expressing neurons are area-specifically distributed within the cerebral cortex of the rat. Neuroscience 81: 321–330.

Binzegger T, Douglas RJ, Martin KA (2004) A quantitative map of the circuit of cat primary visual cortex. J Neurosci 24:8441–8453.

Calabrese V, Mancuso C, Calvani M, Rizzarelli E, Butterfield DA, Stella AM (2007) Nitric oxide in the central nervous system: neuroprotection versus neurotoxicity. Nat Rev Neurosci 8:766–775.

Chen CC, Abrams S, Pinhas A, Brumberg JC (2009) Morphological heterogeneity of layer VI neurons in mouse barrel cortex. J Comp Neurol 512:726–746.

Collins CE, Airey DC, Young NA, Leitch DB, Kaas JH (2010) Neuron densities vary across and within cortical areas in primates. Proc Natl Acad Sci U S A 107:15927–15932.

Dawson TM, Bredt DS, Fotuhi M, Hwang PM, Snyder SH (1991) Nitric oxide synthase and neuronal NADPH diaphorase are identical in brain and peripheral tissues. Proc Natl Acad Sci U S A 88: 7797–7801.

DeFelipe J (1993a) Neocortical neuronal diversity: chemical heterogeneity revealed by colocalization studies of classic neurotransmit-

ters, neuropeptides, calcium-binding proteins, and cell surface molecules. Cereb Cortex 3:273–289.
DeFelipe J (1993b) A study of NADPH diaphorase-positive axonal plexuses in the human temporal cortex. Brain Res 615:342–346.
DeFelipe J (1997) Types of neurons, synaptic connections and chemical characteristics of cells immunoreactive for calbindin-D28K, parvalbumin and calretinin in the neocortex. J Chem Neuroanat 14:1–19.
DeFelipe J (2002) Cortical interneurons: from Cajal to 2001. Prog Brain Res 136:215–238.
DeFelipe J, Fariñas I (1992) The pyramidal neuron of the cerebral cortex: morphological and chemical characteristics of the synaptic inputs. Prog Neurobiol 39:563–607.
DeFelipe J, Jones EG (1988) Cajal on the cerebral cortex. New York: Oxford University Press.
Douglas RJ, Martin KA (2004) Neuronal circuits of the neocortex. Annu Rev Neurosci 27:419–451.
Douglas RJ, Martin KA (2007) Mapping the matrix: the ways of neocortex. Neuron 56:226–238.
Douglas RJ, Martin KA, Whitteridge D (1989) A canonical microcircuit for neocortex. Neural Comput 1:480–488.
Druga R (2009) Neocortical inhibitory system. Folia Biol (Praha) 55:201–217.
Elston GN (2002) Cortical heterogeneity: implications for visual processing and polysensory integration. J Neurocytol 31:317–335.
Elston GN (2003) Cortex, cognition and the cell: new insights into the pyramidal neuron and prefrontal function. Cereb Cortex 13: 1124–1138.
Elston GN, Benavides-Piccione R, Elston A, Zietsch B, DeFelipe J, Manger P, Casagrande V, Kaas JH (2006a) Specializations of the granular prefrontal cortex of primates: implications for cognitive processing. Anat Rec A Discov Mol Cell Evol Biol 288:26–35.
Elston GN, Elston A, Casagrande V, Kaas JH (2005) Pyramidal neurons of granular prefrontal cortex of the galago: complexity in evolution of the psychic cell in primates. Anat Rec A Discov Mol Cell Evol Biol 285:610–618.
Elston GN, Elston A, Freire MAM, Gomes-Leal W, Pereira A Jr, Silveira LCL, Picanço-Diniz CW (2006b) Specialization of pyramidal cell structure in the visual areas V1, V2 and V3 of the South American rodent, Dasyprocta primnolopha. Brain Res 1106:99–110.
Estrada C, DeFelipe J (1998) Nitric oxide-producing neurons in the neocortex: morphological and functional relationship with intraparenchymal microvasculature. Cereb Cortex 8:193–203.
Franca JG, do-Nascimento JL, Picanço-Diniz CW, Quaresma JA, Silva AL (1997) NADPH-diaphorase activity in area 17 of the squirrel monkey visual cortex: neuropil pattern, cell morphology and laminar distribution. Braz J Med Biol Res 30:1093–1105.
Franca JG, Volchan E (1995) NADPH diaphorase histochemistry as a marker for barrels in rat somatosensory cortex. Braz J Med Biol Res 28:787–790.
Franca JG, Volchan E, Jain N, Catania KC, Oliveira RL, Hess FF, Jablonka M, Rocha-Miranda CE, Kaas JH (2000) Distribution of NADPH-diaphorase cells in visual and somatosensory cortex in four mammalian species. Brain Res 864:163–175.
Freire MAM, Franca JG, Picanço-Diniz CW, Pereira A Jr (2005) Neuropil reactivity, distribution and morphology of NADPH diaphorase type I neurons in the barrel cortex of the adult mouse. J Chem Neuroanat 30:71–81.
Freire MAM, Gomes-Leal W, Carvalho WA, Guimarães JS, Franca JG, Picanço-Diniz CW, Pereira A Jr (2004) A morphometric study of the progressive changes on NADPH diaphorase activity in the developing rat's barrel field. Neurosci Res 50:55–66.
Freire MAM, Guimarães JS, Gomes-Leal WG, Pereira A Jr (2009) Pain modulation by nitric oxide in the spinal cord. Front Neurosci 3:175–181.
Freire MAM, Morya E, Faber J, Santos JR, Guimaraes JS, Lemos NAM, Sameshima K, Pereira A, Ribeiro S, Nicolelis MAL (2011) Comprehensive analysis of tissue preservation and recording quality from chronic multielectrode implants. PLoS One 6:e27554.
Freire MAM, Oliveira RB, Picanço-Diniz CW, Pereira A Jr (2007) Differential effects of methylmercury intoxication in the rat's barrel field as evidenced by NADPH diaphorase histochemistry. Neurotoxicology 28:175–181.
Freire MAM, Rocha EG, Oliveira JLF, Guimaraes JS, Silveira LCL, Elston GN, Pereira A, Picanço-Diniz CW (2010) Morphological variability of NADPH diaphorase neurons across areas V1, V2, and V3 of the common agouti. Brain Res 1318:52–63.
Freire MAM, Tourinho SC, Guimarães JS, Oliveira JLF, Picanço-Diniz CW, Gomes-Leal W, Pereira A Jr (2008) Histochemical characterization, distribution and morphometric analysis of NADPH diaphorase neurons in the spinal cord of the agouti. Front Neuroanat 2:2.
Gabbott PL, Bacon SJ (1995) Co-localisation of NADPH diaphorase activity and GABA immunoreactivity in local circuit neurones in the medial prefrontal cortex (mPFC) of the rat. Brain Res 699: 321–328.
Garthwaite J (2008) Concepts of neural nitric oxide-mediated transmission. Eur J Neurosci 27:2783–2802.
Gharbawie OA, Stepniewska I, Qi H, Kaas JH (2011) Multiple parietal-frontal pathways mediate grasping in macaque monkeys. J Neurosci 31:11660–11677.
Gonchar Y, Wang Q, Burkhalter A (2007) Multiple distinct subtypes of GABAergic neurons in mouse visual cortex identified by triple immunostaining. Front Neuroanat 1:3.
Govsa F, Kayalioglu G (1999) Relationship between nicotinamide adenine dinucleotide phosphate-diaphorase-reactive neurons and blood vessels in basal ganglia. Neuroscience 93:1335–1337.
Guimarães JS, Freire MAM, Lima RR, Souza-Rodrigues RD, Costa AM, dos Santos CD, Picanço-Diniz CW, Gomes-Leal W (2009) Mechanisms of secondary degeneration in the central nervous system during acute neural disorders and white matter damage. Rev Neurol 48:304–310.
Hassiotis M, Paxinos G, Ashwell KW (2005) Cyto- and chemoarchitecture of the cerebral cortex of an echidna (Tachyglossus aculeatus). II. Laminar organization and synaptic density. J Comp Neurol 482:94–122.
Hayama T, Ogawa H (1997) Regional differences of callosal connections in the granular zones of the primary somatosensory cortex in rats. Brain Res Bull 43:341–347.
Hoeffding V, Feldman ML (1988) Changes with age in the morphology of the cochlear nerve in rats: light microscopy. J Comp Neurol 276:537–546.
Hope BT, Michael GJ, Knigge KM, Vincent SR (1991) Neuronal NADPH diaphorase is a nitric oxide synthase. Proc Natl Acad Sci U S A 88:2811–2814.
Horton JC, Adams DL (2005) The cortical column: a structure without a function. Philos Trans R Soc Lond B Biol Sci 360:837–862.
Hurdal MK, Stephenson K (2009) Discrete conformal methods for cortical brain flattening. Neuroimage 45:S86–S98.
Iadecola C, Beitz AJ, Renno W, Xu X, Mayer B, Zhang F (1993) Nitric oxide synthase-containing neural processes on large cerebral arteries and cerebral microvessels. Brain Res 606:148–155.
Jacobs B, Schall M, Prather M, Kapler E, Driscoll L, Baca S, Jacobs J, Ford K, Wainwright M, Treml M (2001) Regional dendritic and spine variation in human cerebral cortex: a quantitative golgi study. Cereb Cortex 11:558–571.
Jaeger D (2000) Accurate reconstruction of neuronal morphology. In: Computational neuroscience: realistic modeling for experimentalists (De Schutter E, ed), pp 159–178. Boca Raton, Florida: CRC Press.
Jelinek HF, Fernandez E (1998) Neurons and fractals: how reliable and useful are calculations of fractal dimensions? J Neurosci Methods 81:9–18.
Kaas JH (1983) What, if anything, is SI? Organization of first somatosensory area of cortex. Physiol Rev 63:206–231.

Kaas JH (1987) The organization of neocortex in mammals: implications for theories of brain function. Annu Rev Psychol 38:129–151.
Kaas JH (2005) From mice to men: the evolution of the large, complex human brain. J Biosci 30:155–165.
Kim U, Ebner FF (1999) Barrels and septa: separate circuits in rat barrels field cortex. J Comp Neurol 408:489–505.
Krubitzer LA (1995) The organization of neocortex in mammals: are species differences really so different? Trends Neurosci 18:408–417.
Krubitzer LA (2009) In search of a unifying theory of complex brain evolution. Ann N Y Acad Sci 1156:44–67.
Krubitzer LA, Hunt DL (2007) Captured in the net of space and time: understanding cortical field evolution. In: The evolution of nervous systems in mammals, Vol. IV (Kaas JH, Krubitzer LA, eds), pp 49–72. Oxford: Academic Press.
Kubota Y, Shigematsu N, Karube F, Sekigawa A, Kato S, Yamaguchi N, Hirai Y, Morishima M, Kawaguchi Y (2011) Selective coexpression of multiple chemical markers defines discrete populations of neocortical GABAergic neurons. Cereb Cortex 21:1803–1817.
Lee JE, Ahn CH, Lee JY, Chung ES, Jeon CJ (2004) Nitric oxide synthase and calcium-binding protein-containing neurons in the hamster visual cortex. Mol Cells 18:30–39.
Lee JE, Jeon CJ (2005) Immunocytochemical localization of nitric oxide synthase-containing neurons in mouse and rabbit visual cortex and co-localization with calcium-binding proteins. Mol Cells 19:408–417.
Lüth HJ, Hedlich A, Hilbig H, Winkelmann E, Mayer B (1994) Morphological analyses of NADPH-diaphorase/nitric oxide synthase positive structures in human visual cortex. J Neurocytol 23:770–782.
Mountcastle VB (1997) The columnar organization of the neocortex. Brain 120 (Pt 4):701–722.
Nelson S (2002) Cortical microcircuits: diverse or canonical? Neuron 36:19–27.
Pereira A Jr, Freire MAM, Bahia CP, Franca JG, Picanço-Diniz CW (2000) The barrel field of the adult mouse SmI cortex as revealed by NADPH-diaphorase histochemistry. Neuroreport 11:1889–1892.
Pietrelli A, López-Costa JJ, Goñi R, López EM, Brusco A, Basso N (2011) Effects of moderate and chronic exercise on the nitrergic system and behavioral parameters in rats. Brain Res 1389:71–82.
Remple MS, Henry EC, Catania KC (2003) Organization of somatosensory cortex in the laboratory rat (Rattus norvegicus): evidence for two lateral areas joined at the representation of the teeth. J Comp Neurol 467:105–118.
Rocha EG, Santiago LF, Freire MAM, Gomes-Leal W, Lent R, Houzel JC, Franca JG, Pereira A Jr, Picanço-Diniz CW (2007) Callosal axon arbors in the limb representations of the somatosensory cortex (SI) in the agouti (Dasyprocta primnolopha). J Comp Neurol 500:255–266.
Rockel AJ, Hiorns RW, Powell TP (1980) The basic uniformity in structure of the neocortex. Brain 103:221–244.
Sandell JH (1986) NADPH diaphorase histochemistry in the macaque striate cortex. J Comp Neurol 251:388–397.
Santiago LF, Rocha EG, Freire MAM, Lent R, Houzel JC, Picanço-Diniz CW, Pereira A Jr, Franca JG (2007) The organizational variability of the rodent somatosensory cortex. Rev Neurosci 18:283–294.
Scherer-Singler U, Vincent SR, Kimura H, McGeer EG (1983) Demonstration of a unique population of neurons with NADPH-diaphorase histochemistry. J Neurosci Methods 9:229–234.
Schottler F, Collins JL, Fergus A, Okonkwo D, Kassell NF, Lee KS (1996) Structural interactions between NOS-positive neurons and blood vessels in the hippocampus. Neuroreport 7:966–968.
Schubert D, Kötter R, Staiger JF (2007) Mapping functional connectivity in barrel-related columns reveals layer- and cell type-specific microcircuits. Brain Struct Funct 212:107–119.
Schweitzer L, Renehan WE (1997) The use of cluster analysis for cell typing. Brain Res Protoc 1:100–108.
Shepherd GM (1991) Foundations of the neuron doctrine, p 352. Oxford University Press.
Sholl DA (1953) Dendritic organization in the neurons of the visual and motor cortices of the cat. J Anat 87:387–406.
Somogyi P, Tamás G, Lujan R, Buhl EH (1998) Salient features of synaptic organisation in the cerebral cortex. Brain Res Brain Res Rev 26:113–135.
Spessert R, Layes E (1994) Fixation conditions affect the intensity but not the pattern of NADPH-diaphorase staining as a marker for neuronal nitric oxide synthase in rat olfactory bulb. J Histochem Cytochem 42:1309–1315.
Steinert JR, Chernova T, Forsythe ID (2010) Nitric oxide signaling in brain function, dysfunction, and dementia. Neuroscientist 16:435–452.
Szentágothai J (1978) The neuron network of the cerebral cortex: a functional interpretation. Proc R Soc Lond B Biol Sci 201:219–248.
Thomas E, Pearse AG (1964) The solitary active cells. Histochemical demonstration of damage-resistant nerve cells with a TPN-diaphorase reaction. Acta Neuropathol 27:238–249.
Valtschanoff JG, Weinberg RJ, Kharazia VN, Schmidt HH, Nakane M, Rustioni A (1993) Neurons in rat cerebral cortex that synthesize nitric oxide: NADPH diaphorase histochemistry, NOS immunocytochemistry, and colocalization with GABA. Neurosci Lett 157:157–161.
Vasconcelos N, Pantoja J, Belchior H, Caixeta FV, Faber J, Freire MAM, Cota VR, Anibal de Macedo E, Laplagne DA, Gomes HM, Ribeiro S (2011) Cross-modal responses in the primary visual cortex encode complex objects and correlate with tactile discrimination. Proc Natl Acad Sci U S A 108:15408–15413.
Vincent SR, Johansson O, Hökfelt T, Skirboll L, Elde RP, Terenius L, Kimmel J, Goldstein M (1983) NADPH-diaphorase: a selective histochemical marker for striatal neurons containing both somatostatin- and avian pancreatic polypeptide (APP)-like immunoreactivities. J Comp Neurol 217:252–263.
Wallace MN (1987) Histochemical demonstration of sensory maps in the rat and mouse cerebral cortex. Brain Res 418:178–182.
Welker C, Woolsey TA (1974) Structure of layer IV in the somatosensory neocortex of the rat: description and comparison with the mouse. J Comp Neurol 158:437–453.
Wong-Riley M, Anderson B, Liebl W, Huang Z (1998) Neurochemical organization of the macaque striate cortex: correlation of cytochrome oxidase with Na+K+ATPase, NADPH-diaphorase, nitric oxide synthase, and *N*-methyl-D-aspartate receptor subunit 1. Neuroscience 83:1025–1045.
Woolsey TA (1967) Somatosensory, auditory and visual cortical areas of the mouse. Johns Hopkins Med J 121:91–112.
Woolsey TA, Rovainen CM, Cox SB, Henegar MH, Liang GE, Liu D, Moskalenko YE, Sui J, Wei L (1996) Neuronal units linked to microvascular modules in cerebral cortex: response elements for imaging the brain. Cereb Cortex 6:647–660.
Xiao YM, Diao YC, So KF (1996) A morphological study of neurons expressing NADPH diaphorase activity in the visual cortex of the golden hamster. Brain Behav Evol 48:221–230.
Yan XX, Garey LJ (1997) Morphological diversity of nitric oxide synthesising neurons in mammalian cerebral cortex. J Hirnforsch 38:165–172.
Yan XX, Jen LS, Garey LJ (1996) NADPH-diaphorase-positive neurons in primate cerebral cortex colocalize with GABA and calcium-binding proteins. Cereb Cortex 6:524–529.

(Accepted 15 December 2011)
(Available online 27 December 2011)